JOURNAL OF GEOPHYSICAL RESEARCH: SPACE PHYSICS, VOL. 118, 4176–4188, doi:10.1002/jgra.50239, 2013

Links between the plasmapause and the radiation belt boundaries as observed by the instruments CIS, RAPID, and WHISPER onboard Cluster

F. Darrouzet,[1] V. Pierrard,[1,2] S. Benck,[2] G. Lointier,[3] J. Cabrera,[2] K. Borremans,[1] N. Yu Ganushkina,[4,5] and J. De Keyser[1]

Received 23 July 2012; revised 6 February 2013; accepted 15 March 2013; published 19 July 2013.

[1] In the present work, we study the relations between the position of the plasmapause and the position of the radiation belt boundaries. The Cluster mission offers the exceptional opportunity to analyze those different regions of the inner magnetosphere with identical sensors on multiple spacecraft. We compare the positions of the radiation belt edges deduced from CIS (Cluster Ion Spectrometry) observations (electrons with energy > 2 MeV) with the positions of the plasmapause derived from WHISPER (Waves of HIgh frequency and Sounder for Probing of the Electron density by Relaxation) data (electron plasma frequency). In addition, we compare those results with the edges positions determined from RAPID (Research with Adaptive Particle Imaging Detectors) observations (electrons with energy between 244.1 and 406.5 keV). The period of 1 April 2007 to 31 March 2009 has been chosen for the analysis because at that time Cluster's perigee was located at lower radial distances than during the earlier part of the mission. The perigee was then as close as 2 R_E, deep inside the plasmasphere and the radiation belts. This time period corresponds to a long solar activity minimum. Differences are observed between the radiation belt boundary positions obtained from the two different instruments: The radiation belt positions are related to the energy bands. The results show that the plasmapause position is more variable than the radiation belt boundary positions, especially during small geomagnetic activity enhancements. A correspondence is observed between the plasmapause position determined by WHISPER and the outer edge of the outer radiation belt of energetic electrons (> 2 MeV) observed by CIS. This result is unexpected since previous studies based on other spacecraft observations indicated a correlation between the inner edge of the outer belt and the plasmapause. However, during higher geomagnetic activity time periods, the plasmapause is located closer to the inner boundary of the outer radiation belt. Also, the thickness of the slot region is found to follow the global evolution of the geomagnetic activity.

Citation: Darrouzet, F., V. Pierrard, S. Benck, G. Lointier, J. Cabrera, K. Borremans, N. Yu Ganushkina, and J. De Keyser (2013), Links between the plasmapause and the radiation belt boundaries as observed by the instruments CIS, RAPID and WHISPER onboard Cluster, *J. Geophys. Res. Space Physics*, *118*, 4176–4188, doi:10.1002/jgra.50239.

1. Introduction

[2] The plasmasphere is a torus-like region of dense and cool plasma (density between 10 and 10^4 cm^{-3} and energy of a few eV) surrounding the Earth [*Lemaire and Gringauz*, 1998; *Darrouzet et al.*, 2009a; *Singh et al.*, 2011; *Darrouzet and De Keyser*, 2013]. This region extends out to several Earth radii (R_E) to a boundary known as the plasmapause or the plasmasphere boundary layer [*Carpenter and Lemaire*, 2004]. In a first theoretical formulation, the plasmapause location coincided with the last closed equipotential of the magnetospheric electrostatic field [*Nishida*, 1966; *Brice*, 1967]. More recently, the plasma interchange mechanism has been proposed for the formation of the plasmapause [*Lemaire*, 1974, 2001]. The plasmasphere's configuration, size, shape, and plasma distribution depend sensitively on

[1]Belgian Institute for Space Aeronomy (IASB-BIRA), Brussels, Belgium.
[2]Université Catholique de Louvain, Center for Space Radiations (CSR), Louvain-La-Neuve, Belgium.
[3]Laboratoire de Physique et Chimie de l'Environnement et de l'Espace (LPC2E), Orléans, France.
[4]Department of Atmospheric, Oceanic and Space Sciences (AOSS), University of Michigan, Ann Arbor, Michigan, USA.
[5]Finnish Meteorological Institute (FMI), Earth Observations, Helsinki, Finland.

Corresponding author: F. Darrouzet, Belgian Institute for Space Aeronomy (IASB-BIRA), 3 Avenue Circulaire, 1180 Brussels, Belgium. (Fabien.Darrouzet@aeronomie.be)

2169-9380/13/10.1002/jgra.50239

the recent history of geomagnetic activity. In particular, the plasmasphere can expand to beyond geosynchronous orbit during extended quiet periods, whereas the plasmapause moves earthward, down to McIlwain L [*McIlwain*, 1961] values < 3 R_E, during high geomagnetic activity [e.g., *Goldstein*, 2006, and references therein].

[3] The Earth's radiation belts consist of energetic protons and electrons (energy $E > 100$ keV) that are trapped by the Earth's magnetic field. They have been discovered in 1958 by the Explorer 1 satellite [*Van Allen*, 1959]. The inner radiation belt is located typically between 1 and 2 R_E and contains electrons and protons. It is relatively stable and varies only during intense geomagnetic activity [*Millan and Thorne*, 2007]. The outer radiation belt extends approximately from 4 to 7 R_E and consists mainly of electrons. It is highly dynamic. Its density can vary by several orders of magnitude over a few hours, especially during geomagnetically active times [*Craven*, 1966]. The outer and inner radiation belts are separated from each other by a slot region. It is commonly accepted that this region is formed because energetic electrons are lost due to pitch-angle scattering by VLF (Very Low Frequency) waves, mainly whistler and plasmaspheric hiss [*Lyons et al.*, 1972]. Those waves are commonly observed in the plasmasphere [*Meredith et al.*, 2004; *Golden et al.*, 2012] and their properties are modeled by simulations [*Chen et al.*, 2012]. Thus, the relation between the plasmapause and the radiation belt boundaries is of fundamental importance.

[4] Several studies have analyzed the relation between the radiation belts and the plasmasphere. In particular, pioneering work by *Baker et al.* [2004] showed that radiation belt populations are sensitive to the core plasmasphere distribution and specifically to the position of the plasmapause. Using SAMPEX (Solar Anomalous Magnetospheric Particle EXplorer) observations, these authors reported that the outer Van Allen belt was compressed dramatically by a strong solar storm known as the "Halloween storm": From 1 to 10 November 2003, the center of the outer belt was only 10,000 km from Earth's equatorial surface. At the same time, the plasmasphere, observed by the EUV (Extreme UltraViolet) imager onboard IMAGE (Image for Magnetopause-to-Aurora Global Exploration), was similarly displaced inwards.

[5] Using SAMPEX daily averaged fluxes of 2 – 6 MeV electrons and EUV 10-min global images of the plasmasphere, *Goldstein et al.* [2005] observed for two events how a severe erosion moved the plasmapause inside $L = 2\,R_E$ and how 2–3 days later the outer belt was located where the slot region usually is found. The authors found the inner extent of the outer belt correlated (to within $\delta L \approx 0.1\,R_E$) with the 3.5-day running average of the plasmapause location. They deduced a ≥3.5-day loss time scale from pitch-angle scattering by plasmaspheric hiss and EMIC (ElectroMagnetic Ion Cyclotron) waves. Plasmasphere erosion provides an opportunity for energetic electrons to persist as trapped radiation belt particles.

[6] *Li et al.* [2006] also established a relationship between the position of the plasmapause and the inner edge of the outer radiation belt. They used CRRES (Combined Release and Radiation Effects Satellite) observations and a model for the plasmapause determination, SAMPEX observations for the radiation belts characterization, and a model. They outlined three mechanisms by which the plasmapause may modify the particle fluxes in the outer belt: (i) Pitch-angle scattering of electrons by VLF and EMIC waves outside the plasmapause causing them to precipitate; (ii) modification by the plasmasphere of the characteristics of the ULF (Ultra Low Frequency) waves that diffuse particles radially inward in space and up in energy space; and (iii) creation of a peak flux just outside the plasmasphere from acceleration by VLF chorus, because those waves are strongest just beyond the plasmapause.

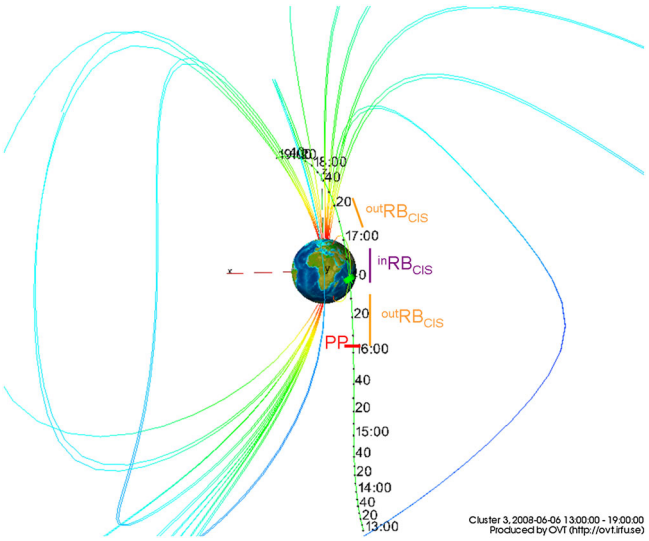

Figure 1. Orbital pass of the Cluster satellite C3 on 6 June 2008 from 13:00 to 19:00 UT projected onto a GSM (Geocentric Solar Magnetospheric) plane. The inbound plasmapause crossing (*PP*) and the outer ($^{out}RB_{CIS}$) and inner ($^{in}RB_{CIS}$) radiation belt locations are indicated in red, orange, and violet, respectively. Figure produced with OVT (Orbit Visualization Tool, http://ovt.irfu.se).

[7] Using SAC-C (Scientific Application Satellite-C) observations, *Pierrard and Benck* [2012] showed that the inward motion of the outer radiation belt associated with injections of energetic electrons during geomagnetic storms follows the plasmapause erosion by several hours. After the storm, the plasmapause moves back to larger radial distances in less than 3 days, while the inner edge of the outer belt remains close to the Earth during more extended periods of several days.

[8] All these results have been obtained by using different satellites and/or models to acquire information about the radiation belts and the plasmapause. The Cluster mission, however, offers the unique opportunity to study both regions with thermal plasma and energetic particle instruments on the same spacecraft, thanks to the large variety of instruments onboard the satellites [*Escoubet et al.*, 1997] and the recent modifications in the orbit. We present the Cluster data analysis in section 2 and the comparison between the boundaries in section 3. Section 4 summarizes the conclusions of this study.

2. Cluster Data Analysis

[9] The Cluster mission consists of four identical spacecraft launched in 2000 on similar elliptical polar orbits with

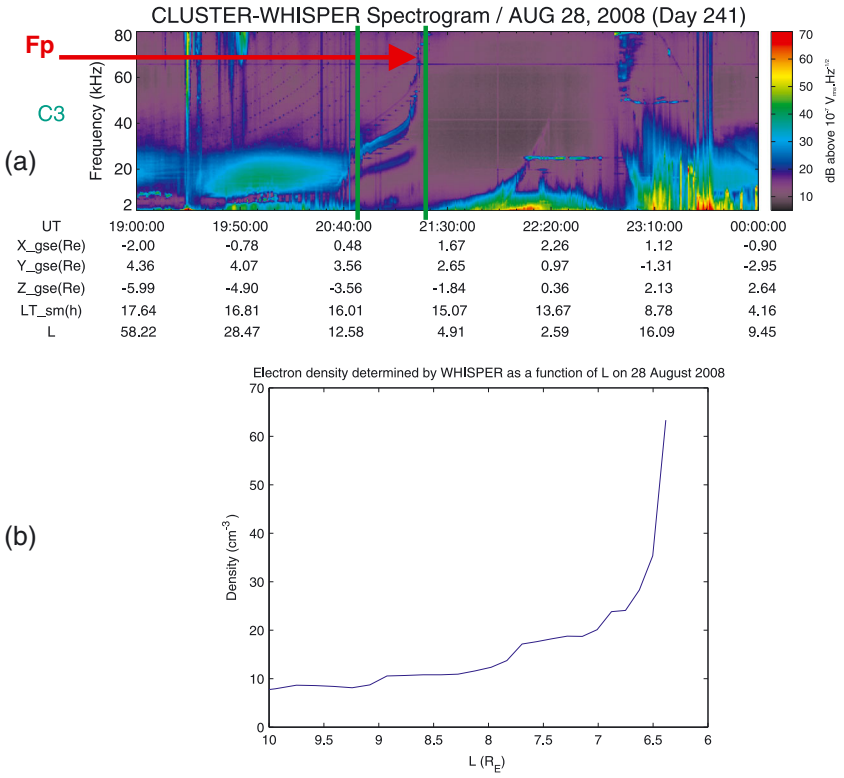

Figure 2. (a) Time-frequency electric field spectrogram measured by WHISPER onboard the Cluster spacecraft C3 on 28 August 2008, between 19:00 and 24:00 UT. The electron plasma frequency *Fp* line is indicated by a red arrow, and the orbital parameters are indicated at the bottom of the panel. (b) Electron density N_e determined from WHISPER measurements onboard C3 as a function of L during the time interval indicated by the green lines in Figure 2a.

an initial perigee at about 4 R_E and an apogee at 19.6 R_E [*Escoubet et al.*, 2001]. Each satellite (C1, C2, C3, and C4) crosses the inner magnetosphere from Southern to Northern Hemisphere around perigee, every 57 h. Due to the annual precession of the orbit, all magnetic local time (MLT) sectors are covered over a year. Each spacecraft carries 11 instruments, allowing the determination of the plasmapause position as well as the locations of the radiation belt boundaries. We use here the WHISPER (Waves of HIgh frequency and Sounder for Probing of Electron density by Relaxation) instrument [*Décréau et al.*, 1997] to analyze the plasmasphere. For the radiation belt characterization, the data sets come from two Cluster instruments: CIS (Cluster Ion Spectrometry) [*Réme et al.*, 1997] and RAPID (Research with Adaptive Particle Imaging Detectors) [*Wilken et al.*, 1997].

[10] We provide an analysis of 2 years of data from 1 April 2007 to 31 March 2009. During this period, the perigee of Cluster was located at lower radial distances than during the first years of the mission. The perigee was as close as 2 R_E, deep inside the plasmasphere and the radiation belts. During the previous years (before 2007), with a perigee located around 4 R_E, the plasmapause was sometimes never encountered, as it is often located at lower radial distances. With such high perigee, the satellites did not cross the radiation belts very often. *Ganushkina et al.* [2011] have used CIS data to determine the boundary locations of the outer and inner radiation belts. For comparison and conformity with this recent study, we have used the same orbital parameters: MLT and L-values were extracted from the CLWeb software (http://clweb.cesr.fr) using the IGRF2000 model for the internal magnetic field and the Tsyganenko T89 model for the external magnetic field [*Tsyganenko*, 1989]. We have used only one Cluster spacecraft, C3, because all three instruments used in this study were functioning well during this time period only onboard this satellite.

[11] Figure 1 presents a typical orbital pass of C3 around perigee as viewed from the Y GSM (Geocentric Solar Magnetospheric) axis and plotted with OVT (Orbit Visualization Tool, http://ovt.irfu.se). This event occurs on 6 June 2008 from 13:00 to 19:00 UT. The inbound plasmapause crossing (from WHISPER) is indicated, as well as the radiation belt locations (from CIS). For this event, the inbound plasmapause crossing occurred around 16:00 UT, when the spacecraft was close to the outer boundary of the outer radiation belt (between 16:00 and 16:30 UT). The inner radiation belt crossing occurred between 16:40 and 16:55 UT as shown in Figure 1. Note that the outer radiation belt is smaller during the outbound pass than during the inbound one in terms of radial width measured along the orbit of the spacecraft. This is mainly due to the Cluster orbit, which is not symmetric around the magnetic equator.

2.1. WHISPER Data Analysis

[12] The WHISPER instrument onboard Cluster allows determining the electron density inside and outside the plasmasphere, as well as the position of the plasmapause [*Décréau et al.*, 2001; *Darrouzet et al.*, 2009b]. WHISPER

provides time-frequency electric field spectrograms during plasmasphere crossings, such as illustrated in Figure 2a for the 28 August 2008, between 19:00 and 24:00 UT, around 15:00 MLT, with $Kp = 3^-$. The WHISPER analysis method consists in finding the electron plasma frequency *Fp* (indicated by a red arrow at the inbound plasmapause crossing in Figure 2a). We analyze the frequency spectra obtained during the passive and active (sounding) operation modes. Several methods can be used to determine *Fp*, for example, the local wave cutoff properties [*Canu et al.*, 2001], the observation of Bernstein modes [*Trotignon et al.*, 2003], or the use of lower hybrid resonances [*Kougblénou et al.*, 2011]. This analysis carries out a direct or indirect determination of N_e related to *Fp* by the relation

$$N_e[\mathrm{cm}^{-3}] = Fp[\mathrm{kHz}]^2/81 \quad (1)$$

[13] The WHISPER instrument can estimate electron densities for values up to 80 cm^{-3} with a temporal resolution of 2 s on average. The uncertainty on the plasma frequency measurements is 163 Hz, which gives a relative error on electron density of the order of 0.5 to 5 % at densities higher than 20 cm^{-3}. We have analyzed only the inbound plasmapause crossings, because the outbound crossings are not as clear due to the presence of many waves (see Figure 2a around 23:10 UT).

[14] For the event displayed on Figure 2a, we plot the density N_e as a function of L in Figure 2b. To determine the plasmapause position, we look for a density increase of at least a factor of 3 over an L-distance of 0.5 R_E or less, with an increase up to a density larger than 20 cm^{-3}. We then consider the location of the upper value of the density ramp to be the position of the plasmapause. There, we can compute all the parameters needed for our statistical analysis. We also take into account the presence of plasmaspheric plumes (using the statistical analysis of plumes observed by Cluster made by [*Darrouzet et al.*, 2008] and recently extended for the years 2007–2009) in order to avoid an erroneous plasmapause determination.

[15] There are a few limitations to this technique. The limit on the maximum electron density that can be measured by the WHISPER instrument (80 cm^{-3}) sometimes prevents a complete determination of the plasmapause position. Also, the satellite does not always fully cross the plasmapause into the plasmasphere. However, as our statistical study excludes the events with small density gradients and small maximum electron density values, we consider that the events selected here give an innermost plasmapause position, not far from the plasmapause position that would be defined as the middle of the plasmasphere boundary layer. In this way, we consider the same plasmapause position as in the study of [*Li et al.*, 2006].

[16] About 200 inbound plasmapause crossings were detected during the 2 years analyzed. The L–MLT probability of occurrence of the plasmapause based on the inbound crossings is shown in Figure 3. The uncertainty on L is between 0.05 and 0.1 R_E, and negligible for MLT (varying very slowly during a single plasmasphere crossing). All MLT sectors are covered except the early morning, mainly due to the solar eclipse season in March–April 2008. The probability of occurrence is on average, similar in all MLT sectors. The L-position of the plasmapause ranges between

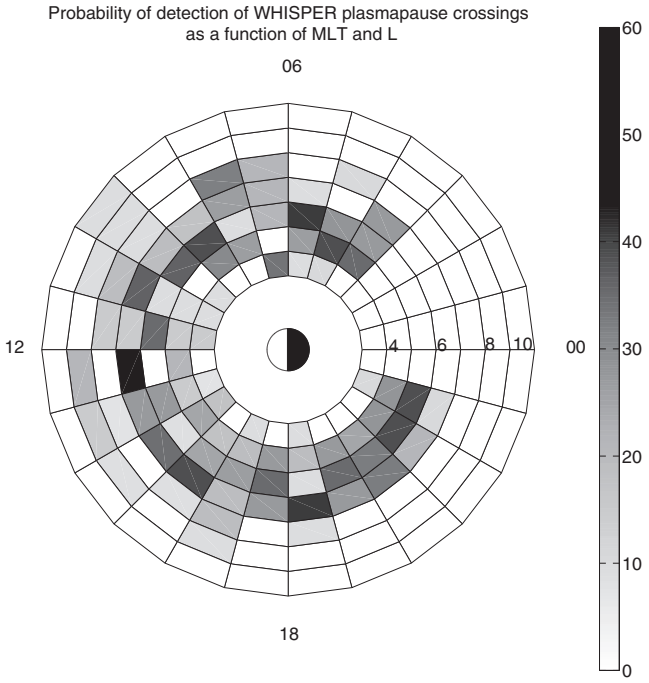

Figure 3. L–MLT probability of occurrence of the plasmapause inferred from inbound crossings and determined by WHISPER onboard C3 from 1 April 2007 to 31 March 2009. L varies between 3 and 10 R_E, and the gray bar indicates the percentage of plasmapause crossings per L–MLT bin.

3.5 and 9 R_E, and mainly between 5 and 7 R_E. This is quite far from the Earth, due to the low geomagnetic activity during this period.

[17] Figure 4 presents the *Dst* variations and plasmapause positions during the 2 years analyzed (1 April 2007–31 March 2009). *Dst* is shown in Figure 4a, in green for all values and in blue for selected times when a plasmapause crossing has been determined from WHISPER observations. Figure 4b shows the plasmapause positions determined from WHISPER data (in red) compared with the positions of the plasmapause predicted (in blue) by the *Dst* relation (equation (2)) of *O'Brien and Moldwin* [2003]

$$L_{\mathrm{pp}} = 6.3 - 1.57\log_{10}|Dst_{\mathrm{min}}| \quad (2)$$

where Dst_{min} is the minimum value of *Dst* in the preceding 24 h.

[18] This time period is quiet with only four instantaneous values of $Dst < -40$ nT. The plasmapause position derived from WHISPER is at higher L than the modeled location, but both have the same variability (clearly seen, for example, during the first months of 2009). The variations with *Dst* are globally similar and consistent, but the position of the observed plasmapause is sometimes quite different from the modeled value. For example, after the small storm in early September 2008 ($Dst \sim -50$ nT), the observed and modeled plasmapause locations are at similar low L-values (below 4 R_E). On the contrary, the plasmasphere is quite extended during quiet periods, as shown in Figure 4b in early June 2008. Those results are in agreement with previous studies using Cluster and IMAGE data [*Pierrard and Cabrera*, 2005; *Pierrard et al.*, 2008].

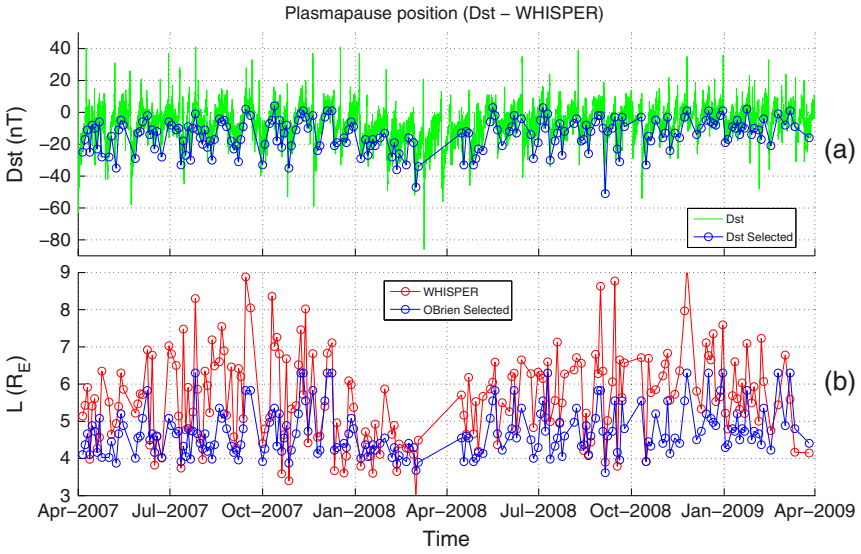

Figure 4. Plasmapause positions determined from WHISPER onboard C3 and from a model from 1 April 2007 to 31 March 2009 and variation of the *Dst* index: (a) Observed *Dst* index (green) and selected values of *Dst* (blue) at the time of the WHISPER plasmapause determination; (b) *L*-positions of the plasmapause derived from WHISPER measurements (red) compared with the ones predicted by the *Dst* relation of *O'Brien and Moldwin* [2003] (blue).

[19] The same analysis has been done with two models that depend on the *Kp* index. We have used relations by *Carpenter and Anderson* [1992] (equation (3)) and by *O'Brien and Moldwin* [2003] (equation (4)), relations depending on the maximum value of *Kp* in the preceding 24 h

$$L_{pp} = 5.6 - 0.46Kp_{max} \quad (3)$$

$$L_{pp} = 5.9 - 0.43Kp_{max} \quad (4)$$

[20] The observed *Kp* is shown in Figure 5a, in green for all values and in blue for selected times when a plasmapause crossing has been determined from WHISPER observations. Figure 5b presents the three plasmapause positions: The observed plasmapause (in red) and the two modeled plasmapauses (in blue and black). This time period is quiet with only 5 instantaneous values of $Kp > 5$. As for *Dst*, the observed plasmapause positions are at higher *L* than the modeled ones, but with similar variations. This difference

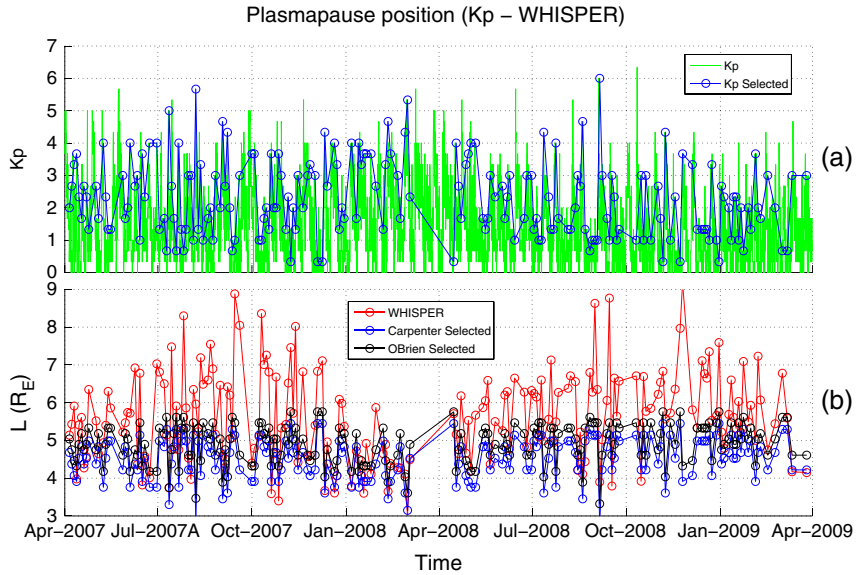

Figure 5. Plasmapause positions determined from WHISPER onboard C3 and from two models from 1 April 2007 to 31 March 2009 and variation of *Kp* index: (a) Observed *Kp* index (green) and selected values of *Kp* (blue) at the time of the WHISPER plasmapause determination; (b) *L*-positions of the plasmapause derived from WHISPER measurements (red) compared with the ones predicted by the *Kp* relation of *Carpenter and Anderson* [1992] (blue), and with the ones predicted by the *Kp* relation of *O'Brien and Moldwin* [2003] (black).

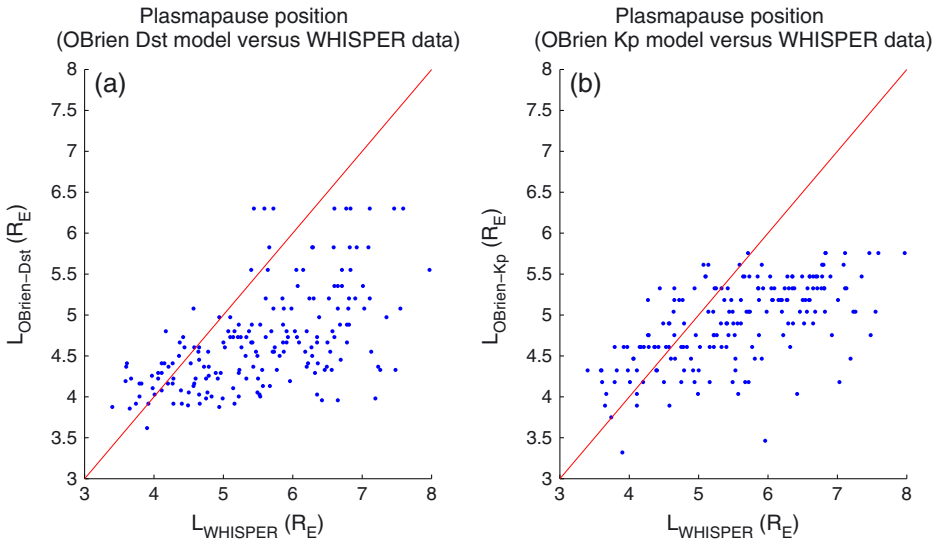

Figure 6. Correlation between plasmapause positions determined from WHISPER onboard C3 and from two models from 1 April 2007 to 31 March 2009: (a) *Dst* dependent model and (b) *Kp* dependent model [*O'Brien and Moldwin*, 2003].

is larger during periods of lower geomagnetic activity. The reason could be that, in such instances, the WHISPER instrument does not record a full crossing of the plasmapause but only its outer boundary, due to the density limitations of the instrument. Also, both models give different results, with a quasi-systematic shift of 0.4 R_E, with the *Carpenter and Anderson* [1992] plasmapause closer to the Earth. One possible reason for this systematic difference is the limited MLT sector coverage used in the data set on which their empirical relation was based.

[21] In order to better bring out the correlations between the satellite data and the models, Figure 6 shows the correlation between plasmapause positions determined from WHISPER and from two models from 1 April 2007 to 31 March 2009. Here, we use only the *Kp* and *Dst* relations from *O'Brien and Moldwin* [2003]. There is a better correlation with the model depending on *Kp*, and the correlation is high only for events with a plasmapause located at $L < 5\ R_E$. Note that there is a considerable scatter between the models and the data, not surprisingly since the same scatter was present for the data in which these empirical models were based [*O'Brien and Moldwin*, 2003].

2.2. CIS Data Analysis

[22] The CIS experiment onboard Cluster consists of two complementary spectrometers: CODIF (COmposition and DIstribution Function) and HIA (Hot Ion Analyzer) [*Réme et al.*, 2001]. CIS provides energy-time spectrograms of ions

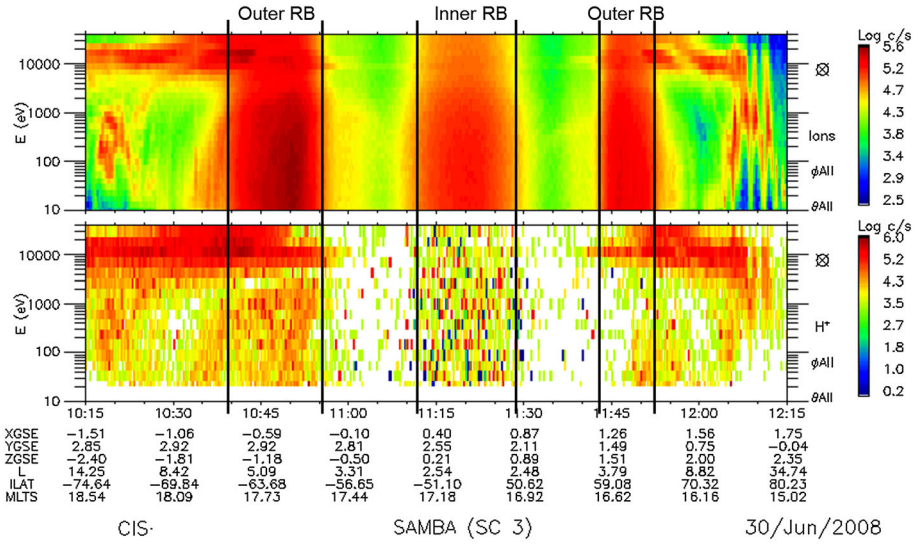

Figure 7. Energy-time spectrograms of ions (in counts/s) observed by CIS onboard C3 on 30 June 2008, between 10:15 and 12:15 UT, at about 16:00–18:00 MLT: HIA ions (top panel) and CODIF H^+ (bottom panel). The locations of the radiation belt boundaries as identified from the detected background are indicated by black vertical lines. Orbital parameters are indicated at the bottom of the figure. (Adapted from *Ganushkina et al.* [2011]).

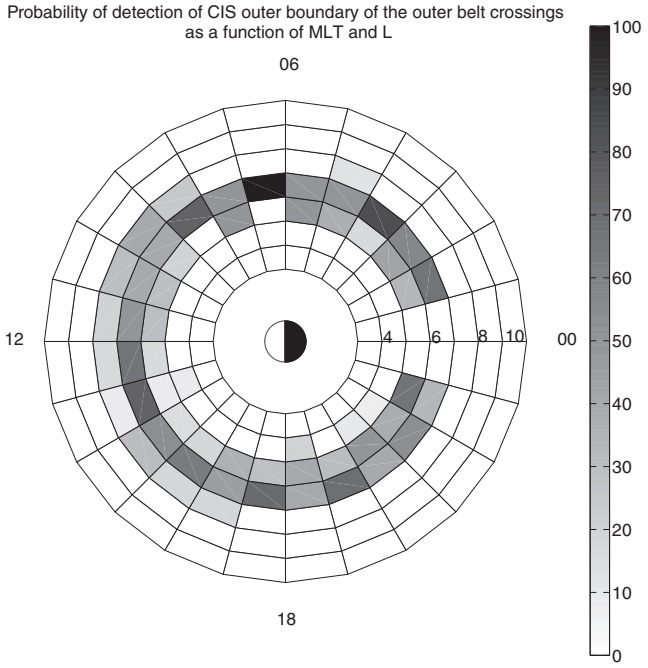

Figure 8. *L*–MLT probability of occurrence of the outer boundary of the outer radiation belt as inferred from inbound crossings and determined by CIS onboard C3 from 1 April 2007 to 31 March 2009. *L* varies between 3 and 10 R_E, and the gray bar indicates the percentage of inbound outer radiation belt crossings per *L*–MLT bin.

(in terms of count/s) during radiation belt crossings. An example is presented in Figure 7 for C3 on 30 June 2008, between 10:15 and 12:15 UT, at about 16:00–18:00 MLT with HIA ions (E = 5 eV–32 keV) shown in the top panel and CODIF H^+ (E = 0.02–40 keV) in the bottom panel. Even if the CIS observations do not contain direct measurements of radiation belt fluxes, the boundaries of the outer and inner radiation belts can be clearly identified from background counts in all energy channels. Those boundaries are illustrated by the black vertical lines in Figure 7. Knowing the shielding parameters of the instruments, the measured background is estimated to be due to electrons with $E > 2$ MeV. The full method to derive the radiation belt boundary positions from CIS measurements is detailed by *Ganushkina et al.* [2011].

[23] *Ganushkina et al.* [2011] provided a complete analysis of CIS data from April 2007 to June 2009 to determine the boundaries of the radiation belts for electrons with $E >$ 2 MeV. By selecting data only between 1 April 2007 and 31 March 2009, we derived the *L*–MLT distribution of the locations of the inner and outer belts boundaries: The outer boundary of the outer radiation belt lies in $L = 5 - 7\,R_E$; the inner boundary of the outer radiation belt is situated in $L = 3 - 4\,R_E$; the outer boundary of the inner radiation belt is found between $L = 2 - 3\,R_E$.

[24] Figure 8 presents the *L*–MLT probability of occurrence of the outer boundary of the inbound outer radiation belt. About 220 crossings were observed during the 2 years analyzed. There are no data in the early morning MLT sector during those 2 years. This is due to the eclipse season in March–April 2008 and an impossibility to determine this boundary from CIS measurements from January to March 2009. There is no MLT dependence. The highest occurrence probability is between 6 and 7 R_E.

[25] The results of this study are used for comparison with data obtained by two other instruments onboard Cluster: WHISPER (see previous section) and RAPID (see next section).

2.3. RAPID Data Analysis

[26] The RAPID experiment onboard Cluster is an advanced particle detector for the analysis of suprathermal plasma distributions in the energy range 20–400 keV for electrons, 40–1500 keV for protons [*Wilken et al.*, 2001]. The instrument consists of two sets of imaging spectrometers, one for electrons and one for ions. Each set is composed of three telescopes, each of which is subdivided internally into 3 or 4 "pixels" for electrons and ions, respectively. The Cluster Active Archive (http://caa.estec.esa.int/caa/home.xml) provides the scientific community with both particle fluxes from RAPID, as well as the count rates, representing the raw data not influenced by any further processing or calibration procedure [*Kronberg and Daly*, 2010]. For this study,

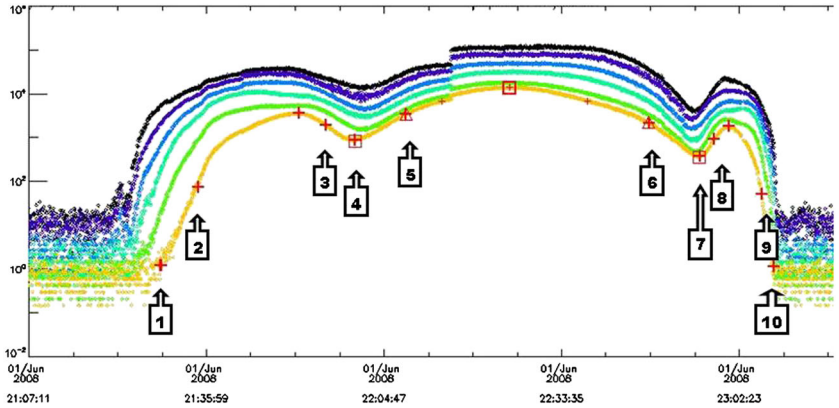

Figure 9. Omni-directional differential fluxes in $cm^{-2}\ s^{-1}sr^{-1}keV^{-1}$ measured by RAPID onboard C3 as a function of time for the radiation belt crossing on 1 June 2008, for six different energy channels (channel 1 in black, channel 2 in violet, channel 3 in blue, channel 4 in turquoise, channel 5 in green, channel 6 in yellow). The boundaries defined in the text are indicated by numbers from 1 to 10.

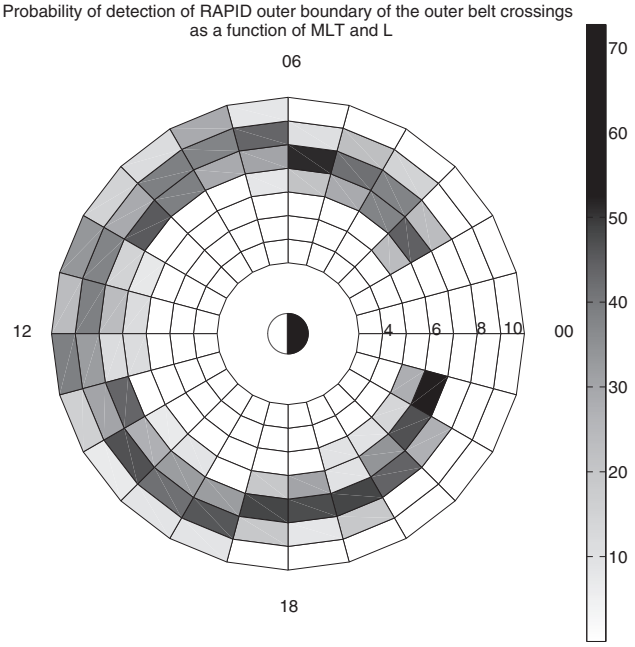

Figure 10. *L*–MLT probability of occurrence of the outer boundary of the outer radiation belt as inferred from inbound crossings (labeled 2 in Figure 9) and determined by RAPID onboard C3 from 1 April 2007 to 31 March 2009. *L* varies between 3 and 10R_E and the gray bar indicates the percentage of inbound outer radiation belt crossings per *L*–MLT bin.

we analyzed specifically the electron omni-directional differential fluxes given in $cm^{-2}s^{-1}sr^{-1}keV^{-1}$ by the sixth energy channel with E = 244.1 – 406.5 keV. Those fluxes are averaged from all detector directions and all spin sectors; they are available at spin resolution all the time (4 s).

[27] Figure 9 displays the analysis window for the electron flux data that is used to extract half-automatically 10 characteristic times, corresponding to 10 radiation belt parameters. The 5 first times concern the inbound crossing:

[28] 1. StartBoundEnterOutRB: Outermost boundary of the outer radiation belt;

[29] 2. OutBoundEnterOutRB: Outer boundary of the outer radiation belt (location where the logarithm of the flux has reached about half of the logarithm of the maximum outer belt flux measured during the inbound crossing);

[30] 3. InBoundEnterOutRB: Inner boundary of the outer radiation belt (mean value of the logarithm of the maximum outer belt flux and the logarithm of the slot region flux measured during the inbound crossing);

[31] 4. CentreEnterSlotRB: Center of the slot region (location of minimum flux attained between the outer and inner radiation belt); and

[32] 5. OutBoundEnterInRB: Outer boundary of the inner belt (mean value of the logarithm of the maximum inner belt flux and the logarithm of the slot region flux measured during the inbound crossing).

The 5 last times correspond to the outbound crossing:

[33] 6. OutBoundExitInRB: Outer boundary of the inner belt (mean value of the logarithm of the maximum inner belt flux and the logarithm of the slot region flux measured during the outbound crossing);

[34] 7. CentreExitSlotRB: Center of the slot region (location of minimum flux attained between the outer and inner radiation belt);

[35] 8. InBoundExitOutRB: Inner boundary of the outer radiation belt (mean value of the logarithm of the maximum outer belt flux and the logarithm of the slot region flux measured during the outbound crossing);

[36] 9. OutBoundExitOutRB: Outer boundary of the outer radiation belt (location where the logarithm of the flux has reached about half of the logarithm of the maximum outer belt flux measured during the outbound crossing); and

[37] 10. StartBoundExitOutRB: Outermost boundary of the outer radiation belt.

[38] The *L*–MLT probability of occurrence of the RAPID outer boundary of the outer belt is presented in Figure 10. The uncertainties on RAPID positions are similar as those for WHISPER (between 0.05 and 0.1 R_E for *L*, negligible for MLT). All MLT sectors are covered by this study containing about 260 boundaries, except around midnight, for the same reasons as for the CIS instrument (not possible to determine the boundaries with the RAPID instrument). The outer boundary of the outer radiation belt is located between 4 and 9 R_E, and most often between 6 and 8 R_E (see Figure 10). The inner boundary of the outer radiation belt is situated around 4.5 R_E, and the outer boundary of the inner radiation belt is located around 3.5 R_E (figures not shown). Those positions are at slightly larger *L*-values than deduced from CIS. This is due to the fact that, for lower energy electrons, the radiation belts extend further out than for higher energy electrons (more details are given in the next section).

[39] An example of the complete analysis of the boundaries found with RAPID is illustrated in Figure 11 for June 2008. The outer radiation belt boundary positions are more variable than those of the inner radiation belt, as observed from previous studies [see *Millan and Thorne*, 2007, for a review]. Even if this month corresponds to a solar minimum activity period, a small geomagnetic activity enhancement occurred on 14 June 2008, where the *Kp* index increased up to 6^-, *Dst* decreased down to –40 nT, and *AE* increased up to almost 1000 nT. After this event, the different radiation belt boundaries clearly moved closer to the Earth. This is mostly the case for the outer boundaries. As a consequence, the slot region is smaller in *L*-size (about 1 R_E before 14 June 2008, around 0.7 R_E during a few days, back at about 1 R_E 10 days later).

3. Results of the Comparison

[40] Figure 12 illustrates the measurements obtained onboard C3 from 1 April 2007 to 31 March 2009 during inbound crossings with the three instruments: The plasmapause position deduced from WHISPER (in black), the inner and outer edges of the outer radiation belt determined from CIS (respectively, in blue and green), and the inner and outer edges of the outer radiation belt determined from RAPID (respectively, in red and magenta). Figure 12a shows the exact values determined at selected times when the boundary was observed and Figure 12b the running averages of those values. Note that we have selected the boundaries as observed during the entrance into the plasmasphere and into the radiation belts, and not during the exit. The main reason is because the inbound plasmapause is usually more clearly seen on the WHISPER spectrograms due to the fact

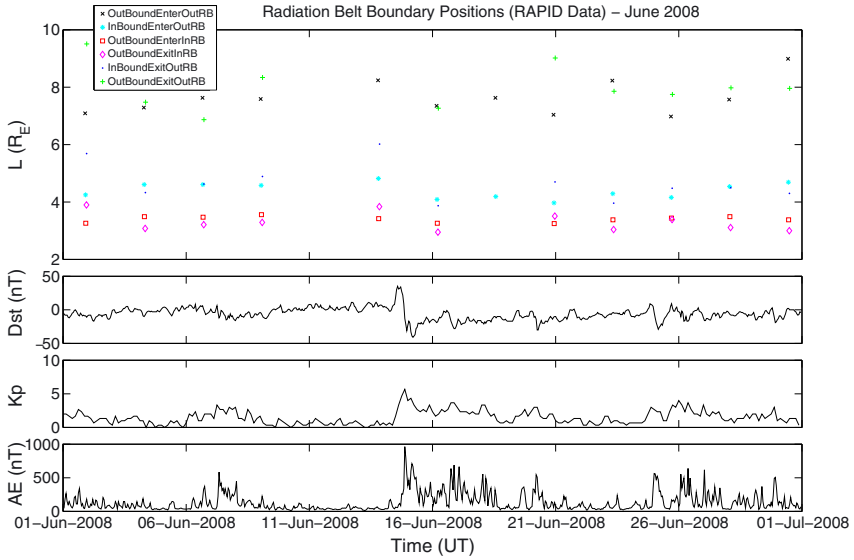

Figure 11. Position of the different radiation belt boundaries for the electron population with E = 244.1–406.5 keV (RAPID data) as a function of time for the month of June 2008 (top panel). The three panels below represent the *Dst*, *Kp*, and *AE*-index evolution during this month.

that the orbit of the spacecraft is more perpendicular to this boundary, and thus easier to detect (see Figure 2a). Also, the radiation belt boundaries are usually more clearly defined during the inbound pass than during the outbound one (figure not shown). There are almost no observations during mid-March to mid-April 2008 and after mid-March 2009, time periods that correspond to midnight MLT. This is mainly due to solar eclipse when the satellite is located behind the Earth and the instruments are switched off. From January 2009, the background counts measured by CIS were very weak, so it makes the determination of radiation belt boundaries quite difficult. This is due to the low geomagnetic activity as well

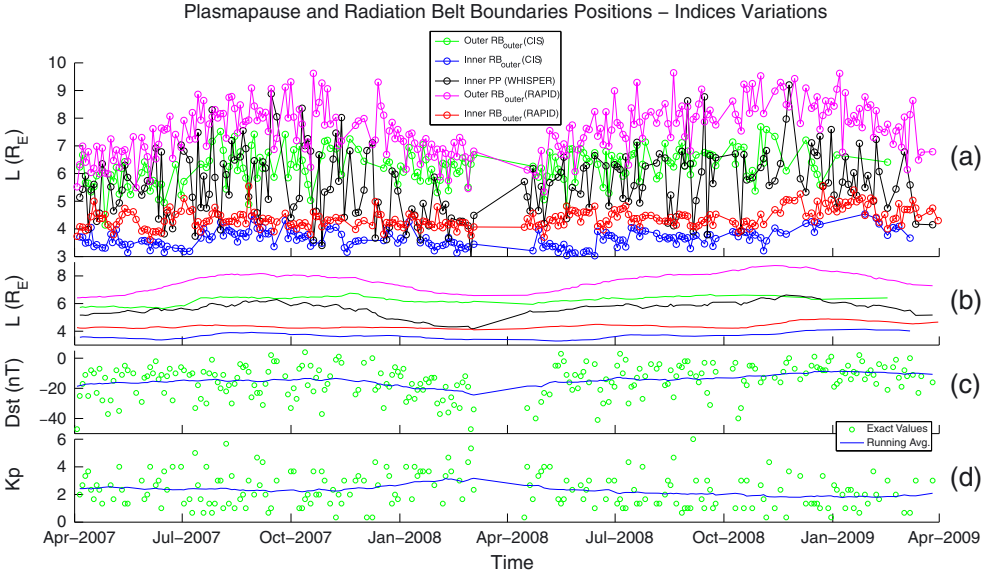

Figure 12. Positions of the plasmapause and outer radiation belt boundaries obtained onboard C3 from 1 April 2007 to 31 March 2009 during inbound crossings: (a) Plasmapause (black) as determined from WHISPER; inner edge (blue), and outer edge (green) of the outer radiation belt as determined from CIS (background electrons of E > 2 MeV); inner edge (red) and outer edge (magenta) of the outer radiation belt as determined from RAPID (electrons of E = 244.1 – 406.5 keV); (b) running averages of the data shown in Figure 12a with the same colors for the lines; (c) minimum values of the *Dst* index in the 24 h preceding an event (green circles) and running averages of those values (blue line); (d) maximum values of the *Kp* index in the 24 h preceding an event (green circles), and running averages of those values (blue line).

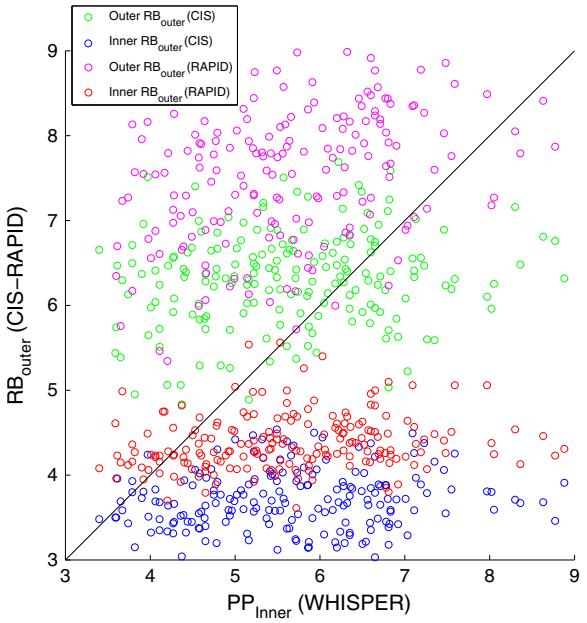

Figure 13. Correlation between plasmapause positions determined from WHISPER and positions of the inner and outer boundaries of the outer radiation belts determined from CIS (green and blue) and RAPID (magenta and red), from 1 April 2007 to 31 March 2009 and during inbound crossings by C3.

as the changing orbit of the Cluster satellites, now crossing the radiation belts at higher magnetic latitudes [*Ganushkina et al.*, 2011].

[41] Globally, there are not many geomagnetic activity variations during this time period (see Figures 12c and 12d). Therefore, it is difficult to see a consistent correlation between them and the radiation belt boundary and plasmapause positions. However, between December 2007 and March 2008, there is a slight increase of geomagnetic activity (as seen for instance in Figure 12d with the slight increase of the *Kp* index). This clearly has an effect on the boundary positions, especially for the outer radiation belt boundary and the plasmapause, which are closer to the Earth (see Figure 12b).

[42] The inner boundary positions of the outer radiation belt are much less variable than those of the outer boundaries (see Figure 12a). This is because the inner boundary responds less quickly and less sensitively to the solar wind and geomagnetic activity variations. By comparing the different data sets, one observes that the plasmapause corresponds rather to the outer boundary of the outer belt of relativistic electrons ($E > 2$ MeV) detected by CIS (see Figure 12b). It only occasionally matches with the inner edge of the outer belt of the 244.1 – 406.5 keV electrons, especially when the plasmapause is closer to the Earth, which corresponds to high geomagnetic activity periods. This is especially the case in January–March 2008, where the *Dst* index has its lower values (see Figure 12c). The plasmapause is also observed to be very dynamic, even during this quiet period. This was expected from the plasmaspheric model developed by *Pierrard and Stegen* [2008], recently coupled to the ionosphere [*Pierrard and Voiculescu*, 2011], that shows that not only magnetic storms but also moderate *Kp* variations can significantly modify the plasmapause position.

[43] There is a shift in the positions of the inner and outer belt boundaries for the two electron populations under consideration: $E > 2$ MeV for CIS and $E = 244.1 – 406.5$ keV for RAPID (see Figure 12b). The inner and outer edges of the belt depend on the considered energy. The higher the electron energy, the less extended is the radiation belt. This is also reproduced by models such as AE8 [*Vette*, 1991]. The edges are located at higher radial distances for lower energy populations than for higher energy. The inner edge of the outer belt for $E > 3$ MeV is located around $3\,R_E$ in the AE8 model. This is clearly closer to the Earth than the plasmapause. The energy range of the considered particles is thus fundamental when considering correlations between radiation belts and plasmapause.

[44] In order to better see the correlations between the boundaries of both regions, we plot the inner and outer

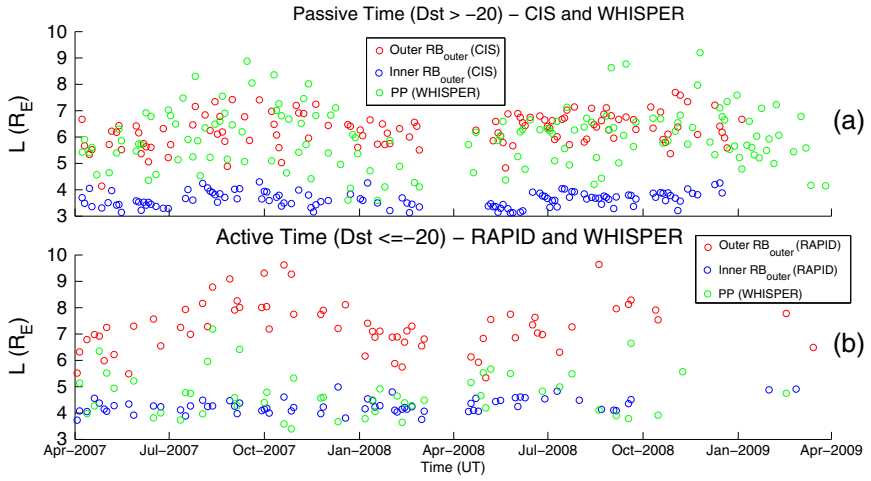

Figure 14. Positions of the plasmapause and outer radiation belt boundaries determined onboard C3 from 1 April 2007 to 31 March 2009 during inbound crossings: Plasmapause (green) as determined from WHISPER, and inner edge (blue) and outer edge (red) of the outer radiation belt as determined (a) from CIS for high *Dst* index and (b) from RAPID for low *Dst* index.

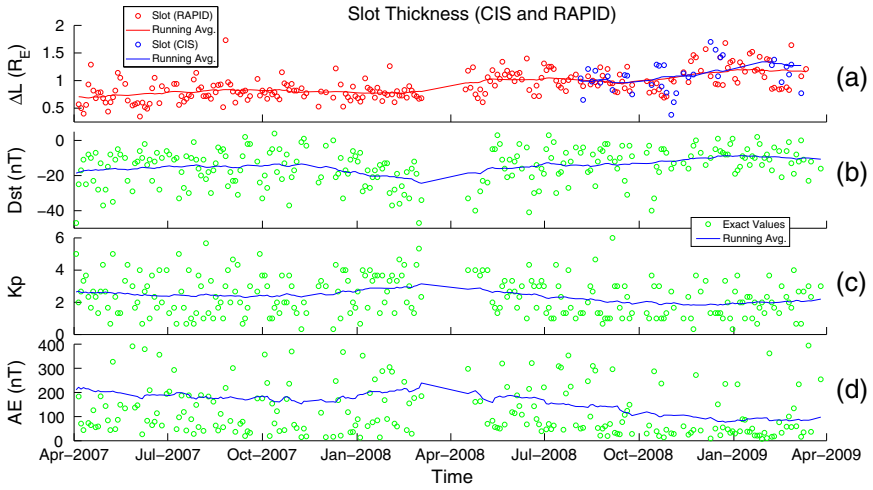

Figure 15. (a) Thickness ΔL of the slot region determined from CIS (blue circles) and RAPID (red circles) data taken onboard C3 from 1 April 2007 to 31 March 2009 during the inbound crossings of the radiation belts. Running averages of those values are plotted as solid lines with the same colors. (b–d) Variations of the indices *Dst*, *Kp*, and *AE* during this period of time (green circles) and running averages of those values (blue lines).

boundary positions of the outer radiation belt against the plasmapause position in Figure 13. We clearly observe the shift between CIS and RAPID data, with the outer radiation belt closer to the Earth for the higher energy ions measured by CIS. The plasmapause derived from WHISPER is near the inner boundary when it is closer to the Earth ($L < 4.5\,R_E$), that is, in case of high geomagnetic activity. For a plasmasphere extending beyond $L > 6.5\,R_E$ (case of lower geomagnetic activity), the plasmapause is closer to the outer boundary. This has also been shown with SAMPEX data by *Li et al.* [2006]: Only the initial penetration of the outer boundary into the inner magnetosphere upon a geomagnetic event follows the plasmapause erosion; afterwards, the plasmapause moves outward and towards the outer boundary, the high energy electrons stay at low L and the inner boundary does not follow the plasmapause.

[45] While this study covers a time period of minimum solar activity, there were some time periods with a certain geomagnetic activity (as seen in Figure 12). We divide our data set by analyzing the minimum *Dst* index in the 24 h preceding an event and by distinguishing data with *Dst* more and less than –20 nT. The plasmapause positions (from WHISPER) and the outer radiation belt boundary positions (from CIS and RAPID) are then studied and shown in Figure 14. During very quiet times (Figure 14a), the plasmapause is located around $L = 6\,R_E$, in the middle of the outer belt, but closer to the outer boundary. During more active times (Figure 14b), the plasmapause moves closer to the Earth ($L = 4 – 5\,R_E$), near the inner boundary of the outer belt. This last result is in agreement with previous studies [e.g., *Goldstein et al*., 2005]. The outer boundary position (red circles) is more variable than the inner one (blue circles), even during quiet times, because it responds more quickly and sensitively to the variations in the solar wind and geomagnetic activity. Moreover, the outer boundary is more variable during the most active times, even if those time periods are not very active in absolute terms (lowest *Dst* is –50 nT).

[46] In this study, we have compared instantaneous observations of two regions of the inner magnetosphere with three different instruments onboard the same satellite. In particular, the WHISPER analysis gives us a local determination of the plasmapause position rather than a global one. Knowing that the plasmapause shape is often irregular and changing with local time, we cannot give a formal conclusion about the global shape and position of the plasmapause. Those limitations in our study do not allow us to draw definitive conclusions about the mechanisms of coupling between the plasmasphere and the radiation belts, in particular the mechanisms forming the slot region. Moreover, due to the Cluster orbital period, our observations are available every 2.5 days at best, and this does not allow us to compute plasmapause positions averaged over a few days, as in previous studies [*Goldstein et al.*, 2005; *Li et al.*, 2006].

[47] The outer boundaries of the inner radiation belt are determined not only from CIS (see Figure 7) but also from RAPID data (see Figure 9). It is therefore possible to compute the thickness ΔL of the slot region between those boundaries and the inner boundaries of the outer belt. As previously, we have analyzed only the radiation belt crossings during the inbound passes. Figure 15 presents the evolution of ΔL as a function of time. For the CIS data, it was possible to do such an analysis only after August 2008. During this common time period, the two data sets give very similar slot thickness values and variations (increasing with time). For the RAPID data, there are clearly two different time periods, one before March 2008 and one after May 2008. During the first time period, ΔL is quite constant between 0.8 and 1.0 R_E, with a geomagnetic activity quite low and constant. After May 2008, ΔL is slowly increasing from 1.0 to 1.2 R_E. This is clearly related to the evolution of the geomagnetic activity as seen from the *Kp* and *AE* indices (see Figures 15c and 15d), which are decreasing progressively during this time period (for example, the average *AE* is varying from 200 nT in June 2008 to 100 nT in March 2009). This thickness increase is mainly due to the variation of the inner boundary of the outer

radiation belt, whose position is also increasing during this low geomagnetic activity time period. During this time, the position of the outer boundary of the inner belt is not varying much.

4. Conclusions

[48] During the period 1 April 2007–31 March 2009, the Cluster spacecraft penetrated deep inside the plasmasphere and the radiation belts since the perigee descended as low as $2\,R_E$. We analyzed the electron populations at different energies as observed by three instruments onboard the Cluster satellite C3:

The plasmasphere (cold 1 eV electrons) with WHISPER;
The radiation belt (electrons with $E > 2$ MeV) with CIS; and
The radiation belt (electrons with $E = 244.1$–406.5 keV) with RAPID.

[49] The period 2007–2009 corresponds to a long period of solar minimum activity. The geomagnetic activity level is quite small ($Dst < -40$ nT only four times). Due to this low activity, the plasmasphere extends beyond $L > 5\,R_E$. The plasmapause position is observed to be very sensitive to geomagnetic activity, even for small variations. The radiation belts were also very weak during this period.

[50] From the analysis of Cluster observations, it appears that during prolonged geomagnetically quiet periods, the plasmapause coincides more with the outer boundary of the very energetic electrons ($E > 2$ MeV) than with the inner boundary of the radiation belts. The same result has been shown by *Li et al.* [2006], with the inner edge of the outer belt not following the plasmapause all the time after its erosion. The radiation belt population coexists with the plasmasphere during this period out to large radial distances. The plasmasphere population does not seem to play a role in the diffusion of the more energetic particles. But during small geomagnetic activity enhancements, the plasmapause moves closer to the inner boundary of the outer belt, as shown before by *Goldstein et al.* [2005]. Daily variations in the positions of the radiation belt boundaries and plasmapause are often similar, but some differences appear in the different electron populations of the radiation belts (as seen from CIS and RAPID observations).

[51] The radiation belt boundary positions are related to the energy bands. In our analysis, we use two instruments based on different measurement methods and with two different energy bands. Relations between radiation belt boundary positions and the plasmapause thus are specific for the radiation belt particle energies considered.

[52] When the geomagnetic activity is decreasing (as seen from the evolution of the *Kp* and *AE* indices), the thickness of the slot is increasing.

[53] Since the analyzed period did not include a significant geomagnetic storm, a larger database of plasmapause positions covering different geomagnetic activity levels and especially including geomagnetic storms would be useful to complete the comparison. This will be possible in the future since the level of geomagnetic activity started to increase in 2011, and the Cluster mission continues to provide new and accurate observations.

[54] **Acknowledgments.** The *Kp*, *Dst*, and *AE* indices were provided by the Space Environment Information System, SPENVIS (http://www.spenvis.oma.be). F. Darrouzet and J. De Keyser thank ESA for the Cluster mission and the Belgian Federal Science Policy Office (Belspo) through a Prodex project (contract 13127/98/NL/VJ). F. Darrouzet, J. De Keyser, and V. Pierrard acknowledge BISA (Belgian Institute for Space Aeronomy), STCE (Solar-Terrestrial Center of Excellence), and Belspo for their support. V. Pierrard and K. Borremans thank the funding from the European Commission's Seventh Framework Program (FP7/2007-2013) inside the grant agreement SWIFF (project 2633430). J. Cabrera and S. Benck acknowledge Belspo through a Prodex project (contract 90353). N. Ganushkina gratefully acknowledges the support by Observatoire Midi-Pyrénées (poste rouge). N. Ganushkina's work was also partly supported by the Academy of Finland and NASA and NSF grants. The authors thank J. Allard for his contribution in the analysis of some WHISPER observations. The authors thank E. Penou for the development of the CLWeb software.

[55] Masaki Fujimoto thanks the reviewers for their assistance in evaluating this paper.

References

Baker, D. N., S. G. Kanekal, X. Li, S. P. Monk, J. Goldstein, and J. L. Burch (2004), An extreme distortion of the Van Allen belt arising from the "Halloween" solar storm in 2003, *Nature*, *432*(7019), 878–881, doi:10.1038/nature03116.

Brice, N. M. (1967), Bulk motion of the magnetosphere, *J. Geophys. Res.*, *72*(21), 5193–5211, doi:10.1029/JZ072i021p05193.

Canu, P., et al. (2001), Identification of natural plasma emissions observed close to the plasmapause by the Cluster-Whisper relaxation sounder, *Ann. Geophys.*, *19*(10/12), 1697–1709, doi:10.5194/angeo-19-1697-2001.

Carpenter, D. L., and R. R. Anderson (1992), An ISEE/Whistler model of equatorial electron density in the magnetosphere, *J. Geophys. Res.*, *97* (A2), 1097–1108, doi:10.1029/91JA01548.

Carpenter, D. L., and J. Lemaire (2004), The Plasmasphere Boundary Layer, *Ann. Geophys.*, *22*(12), 4291–4298, doi:10.5194/angeo-22-4291-2004.

Chen, L., J. Bortnik, W. Li, R. M. Thorne, and R. B. Horne (2012), Modeling the properties of plasmaspheric hiss: 1. Dependence on chorus wave emission, *J. Geophys. Res.*, *117*, A05201, doi:10.1029/2011JA017201.

Craven, J. D. (1966), Temporal variations of electron intensities at low altitudes in the outer radiation zone as observed with satellite Injun 3, *J. Geophys. Res.*, *71*(23), 5643–5663, doi:10.1029/JZ071i023p05643.

Darrouzet, F., and J. De Keyser (2013), The dynamics of the plasmasphere: Recent results, *J. Atmos. Solar-Terr. Phys. 99*, 53–60, doi:10.1016/j.jastp.2012.07.004.

Darrouzet, F., J. De Keyser, P. M. E. Décréau, F. El Lemdani-Mazouz, and X. Vallières (2008), Statistical analysis of plasmaspheric plumes with CLUSTER/WHISPER observations, *Ann. Geophys.*, *26*(8), 2403–2417, doi:10.5194/angeo-26-2403-2008.

Darrouzet, F., J. De Keyser, and V. Pierrard (eds.) (2009a), *The Earth's Plasmasphere: A Cluster and Image Perspective*, 296 pp., Springer, New York.

Darrouzet, F., et al. (2009b), Plasmaspheric density structures and dynamics: Properties observed by the CLUSTER and IMAGE missions, *Space Sci. Rev.*, *145*(1-2), 55–106, doi:10.1007/s11214-008-9438-9.

Décréau, P. M. E., et al. (1997), WHISPER, a resonance sounder and wave analyser: Performances and perspectives for the Cluster mission, *Space Sci. Rev.*, *79*(1-2), 157–193, doi:10.1023/A:1004931326404.

Décréau, P. M. E., et al. (2001), Early results from the Whisper instrument on Cluster: An overview, *Ann. Geophys.*, *19*(10-12), 1241–1258, doi:10.5194/angeo-19-1241-2001.

Escoubet, C. P., C. T. Russell, and R. Schmidt (eds.) (1997), *The Cluster and Phoenix Missions*, 658 pp., Kluwer Academic Publishers, Dordrecht.

Escoubet, C. P., M. Fehringer, and M. Goldstein (2001), The Cluster mission, *Ann. Geophys.*, *19*(10-12), 1197–1200, doi:10.5194/angeo-19-1197-2001.

Ganushkina, N. Y., I. Dandouras, Y. Y. Shprits, and J. Cao (2011), Locations of boundaries of outer and inner radiation belts as observed by Cluster and Double Star, *J. Geophys. Res.*, *116*, A09234, doi:10.1029/2010JA016376.

Golden, D. I., M. Spasojevíc, W. Li, and Y. Nishimura (2012), Statistical modeling of in situ hiss amplitudes using ground measurements, *J. Geophys. Res.*, *117*, A05218, doi:10.1029/2011JA017376.

Goldstein, J. (2006), Plasmasphere response: Tutorial and review of recent imaging results, *Space Sci. Rev.*, *124*(1), 203–216, doi:10.1007/s11214-006-9105-y.

Goldstein, J., S. G. Kanekal, D. N. Baker, and B. R. Sandel (2005), Dynamic relationship between the outer radiation belt and the plasmapause during March-May 2001, *Geophys. Res. Lett.*, *32*, L15104, doi:10.1029/2005GL023431.

Kougblénou, S., G. Lointier, P. M. E. Décréau, J.-G. Trotignon, J.-L. Rauch, X. Vallières, P. Canu, A. Masson, and J. Pickett (2011), Lower hybrid resonances stimulated by the four CLUSTER relaxation sounders deep inside the plasmasphere: Observations and inferred plasma characteristics, *Ann. Geophys.*, *29*(11), 2003–2018, doi:10.5194/angeo-29-2003-2011.

Kronberg, E. E., and P. W. Daly, (2010), Calibration report of the RAPID measurements in the Cluster Active Archive (CAA), *Tech. Rep. CAA-EST-CR-RAP*, Max-Planck-Institut für Sonnensystemforschung, Katlenburg-Lindau, Germany.

Lemaire, J. F. (1974), The "Roche-Limit" of ionospheric plasma and the formation of the plasmapause, *Planet. Space Sci.*, *22*(5), 757–766, doi:10.1016/0032-0633(74)90145-7.

Lemaire, J. F. (2001), The formation of the light-ion-trough and peeling off the plasmasphere, *J. Atmos. Solar-Terr. Phys.*, *63*(11), 1285–1291, doi:10.1016/S1364-6826(00)00232-7.

Lemaire, J. F., and K. I. Gringauz (1998), *The Earth's Plasmasphere*, 372 pp., Cambridge University Press, New York.

Li, X., D. N. Baker, T. P. O'Brien, L. Xie, and Q. G. Zong (2006), Correlation between the inner edge of outer radiation belt electrons and the innermost plasmapause location, *Geophys. Res. Lett.*, *33*, L14107, doi:10.1029/2006GL026294.

Lyons, L. R., R. M. Thorne, and C. F. Kennel (1972), Pitch-angle diffusion of radiation belt electrons within the plasmasphere, *J. Geophys. Res.*, *77*(19), 3455–3474, doi:10.1029/JA077i019p03455.

McIlwain, C. E. (1961), Coordinates for mapping the distribution of magnetically trapped particles, *J. Geophys. Res.*, *66*(11), 3681–3691, doi:10.1029/JZ066i011p03681.

Meredith, N. P., R. B. Horne, R. M. Thorne, D. Summers, and R. R. Anderson (2004), Substorm dependence of plasmaspheric hiss, *J. Geophys. Res.*, *109*, A06209, doi:10.1029/2004JA010387.

Millan, R. M., and R. M. Thorne (2007), Review of radiation belt relativistic electron losses, *J. Atmos. Solar-Terr. Phys.*, *69*(3), 362–377, doi:10.1016/j.jastp.2006.06.019.

Nishida, A. (1966), Formation of plasmapause, or magnetospheric plasma knee, by the combined action of magnetospheric convection and plasma escape from the tail, *J. Geophys. Res.*, *71*(23), 5669–5679, doi:10.1029/JZ071i023p05669.

O'Brien, T. P., and M. B. Moldwin (2003), Empirical plasmapause models from magnetic indices, *Geophys. Res. Lett.*, *30*(4), 1152, doi:10.1029/2002GL016007.

Pierrard, V., and S. Benck (2012), The dynamics of the terrestrial radiation belts and its links to the plasmasphere, *AIP Conference Proceedings*, *1500*(1), 216–221, doi:10.1063/1.4768769.

Pierrard, V., and J. Cabrera (2005), Comparisons between EUV/IMAGE observations and numerical simulations of the plasmapause formation, *Ann. Geophys.*, *23*(7), 2635–2646, doi:10.5194/angeo-23-2635-2005.

Pierrard, V., and K. Stegen (2008), A three-dimensional dynamic kinetic model of the plasmasphere, *J. Geophys. Res.*, *113*, A10209, doi:10.1029/2008JA013060.

Pierrard, V., and M. Voiculescu (2011), The 3D model of the plasmasphere coupled to the ionosphere, *Geophys. Res. Lett.*, *38*, L12104, doi:10.1029/2011GL047767.

Pierrard, V., G. V. Khazanov, J. Cabrera, and J. Lemaire (2008), Influence of the convection electric field models on predicted plasmapause positions during magnetic storms, *J. Geophys. Res.*, *113*, A08212, doi:10.1029/2007JA012612.

Rème, H. et al. (1997), The Cluster Ion Spectrometry (CIS) experiment, *Space Sci. Rev.*, *79*(1-2), 303–350, doi:10.1023/A:1004929816409.

Rème, H. et al. (2001), First multi-spacecraft ion measurements in and near the Earth's magnetosphere with the identical Cluster Ion Spectrometry (CIS) experiment, *Ann. Geophys.*, *19*(10-12), 1303–1354, doi:10.5194/angeo-19-1303-2001.

Singh, A., R. Singh, and D. Siingh (2011), State studies of Earth's plasmasphere: A review, *Planet. Space Sci.*, *59*(9), 810–834, doi:10.1016/j.pss.2011.03.013.

Trotignon, J. G., P. M. E. Décréau, J. L. Rauch, E. Le Guirriec, P. Canu, and F. Darrouzet (2003), The Whisper relaxation sounder onboard Cluster: A powerful tool for space plasma diagnosis around the Earth, *Cosmic Res.*, *41*(4), 345–348.

Tsyganenko, N. (1989), A magnetospheric magnetic field model with a warped tail current sheet, *Planet. Space Sci.*, *37*(1), 5–20, doi:10.1016/0032-0633(89)90066-4.

Van Allen, J. A. (1959), Radiation belts around the Earth, *Sci. Am.*, *200*(3), 39–47.

Vette, J. I., (1991), The AE-8 trapped electron model environment, *NASA STI/Recon Technical Report N, 92.*

Wilken, B., et al. (1997), RAPID - The imaging energetic particle spectrometer on Cluster, *Space Sci. Rev.*, *79*(1-2), 399–473, doi:10.1023/A:1004994202296.

Wilken, B., et al. (2001), First results from the RAPID imaging energetic particle spectrometer on board Cluster, *Ann. Geophys.*, *19*(10-12), 1355–1366, doi:10.5194/angeo-19-1355-2001.